Size effects in shape memory alloy microwires

Citation: Chen, Ying, and Christopher A. Schuh. "Size Effects in Shape Memory Alloy Microwires." Acta Materialia 59, no. 2 (January 2011): 537–553.

As Published: http://dx.doi.org/10.1016/j.actamat.2010.09.057

Publisher: Elsevier

Persistent URL: http://hdl.handle.net/1721.1/102373

Version: Author's final manuscript: final author's manuscript post peer review, without publisher's formatting or copy editing

Size effects in shape memory alloy microwires

Ying Chen, Christopher A. Schuh[1]

Department of Materials Science and Engineering, Massachusetts Institute of Technology, 77 Massachusetts Avenue, Cambridge, MA 02139, USA

Abstract

In shape memory alloys, the reversible phase transformations between austenite and martensite give rise to superelasticity and shape memory properties. Here we systematically study the sample size dependence of these properties and the associated transformations in polycrystalline shape memory alloy microwires with a bamboo grain structure, i.e., where the wire diameter is completely spanned by individual grains. Cu-Al-Ni wires with diameters ranging from ~500 down to ~20 microns are fabricated by the Taylor liquid processing technique, and are characterized by both isothermal uniaxial tensile testing and mechanically-constrained thermal cycling. We observe size effects in both the transformation stresses and temperatures. What is more, we find that the stress hysteresis in a mechanical cycle, and the temperature hysteresis in a thermal cycle, both increase with decreasing wire diameter, particularly for wires smaller than 100 microns. A direct consequence of the increased hysteresis is enhanced energy dissipation (i.e., damping capacity) in smaller wires. We also discuss possible physical origins of the observed size effects, including interface and surface energies, stored elastic energy, heat transfer, and internal friction.

[1] Corresponding author. *Email address:* schuh@mit.edu (C.A. Schuh).

1. Introduction

The unique properties of shape memory alloys (SMAs) originate from the diffusionless solid-state phase transformations between austenite, a cubic phase, and martensite, a phase of lower symmetry [1]. A thorough understanding of the size-scale dependence of these transformations is required for modern applications of SMAs in sensing, actuation, impact absorption and damping, energy conversion, smart microdevices, etc., as size effects are critical to the design and reliability of potential micro- and nano-scale devices that employ SMAs. There are two potential size scales that may impact the transformation behavior of SMAs: the grain size d and the sample size D. However, the volume of existing work on the effect of either of these variables in SMAs remains small, probably because processing and characterization of SMAs are both challenging, especially in confined volumes. There is thus a standing scientific and technological need for systematic investigations of size effects in SMAs.

Grain size effects have been primarily studied for the case where the grain size d is considerably finer than the sample size D. The forward transformation from austenite to martensite can be induced by lowering the temperature, in which case the transformation starts at the temperature M_s, or by applying a stress, when the transformation starts at the stress σ_{Ms} (which in the literature is often referred to as σ_c, and is defined in Fig. 1). Prior measurements have shown that M_s is generally independent of d when it is greater than 100 μm, but decreases when d decreases below ~100 μm in bulk polycrystalline Fe-Ni-C [2-5], Fe-Pd [6], Cu-Zn-Al [7], Cu-Al-Ni [8], and Cu-Al-Mn SMAs [9]. Waitz et al. [10, 11] reported that the transformation temperatures continue to decrease with decreasing d in nanocrystalline Ni-Ti SMAs, until d reaches a critical size around 50 nm where transformation to martensite is no longer observed. σ_{Ms} increases with a decreasing ratio d/D in Cu-Al-Ni [12], Cu-Al-Mn [13], Cu-Al-Be [14, 15], Cu-Zn-Al [16], Cu-Zn-Sn [17], and Ti-Ni-Zr [18] sheets or wires with a thickness or diameter D on the millimeter scale [12-18]. In all these cases, the decrease in M_s and increase in σ_{Ms} both suggest that martensite formation is suppressed at smaller relative grain sizes, which reflects increasing grain constraint that apparently opposes the nucleation of martensite from the austenite matrix. A suppression of shape memory under increasing grain constraints has also been observed recently in Ni-Ti films with nanoscale thickness [19].

Thermally-induced reverse transformation from martensite back to austenite finishes at the temperature A_f during heating. A_f has been found to decrease in Fe-Pd SMAs [6], but increase slightly in Cu-Zn-Sn SMAs [17], with decreasing grain size d. The corresponding stress for the mechanically-induced transformation, σ_{Af}, has, however, not been studied in terms of its grain size dependency. This seems to be primarily because most alloys that exhibit size effects in σ_{Ms} are susceptible to intergranular fracture during martensitic transformation in polycrystalline forms. Even if fracture does not occur, the strain recovery during unloading usually decays as d decreases [8, 12, 13, 17], making it difficult to measure σ_{Af}. In the rare cases where the loading and unloading curves can form a closed hysteresis loop similar to that

schematized in Fig. 1(b), it is of great interest to determine the superelastic energy dissipation or damping. Direct measures of the energy dissipation include $\Delta E/E$, with ΔE the area within the hysteresis loop and E the maximum strain energy, and $\tan\phi$, where ϕ is the loss angle and $\tan\phi = \Delta E / 2\pi E$. Araya et al. [15] showed that in Cu-Al-Be wires with D = 0.5 mm, $\Delta E/E$ remains nearly constant when d decreases from ~300 to ~100 μm, but starts to decline below this point. A similar size effect is observed in Cu-Al-Mn sheets [20] and wires [21], where $\tan\phi$ decreases with decreasing d/D. Such decrease in damping at smaller d/D is attributed to three-dimensional grain constraint [20, 21]. Conversely, when d approaches D, the constraint is considerably released, leading to an increase in $\tan\phi$. The highest damping is observed when $d = D$, i.e., in sheets with a columnar grain structure, or in wires with a bamboo grain structure.

Such special SMA geometries with $d = D$ permit consideration of the effect of sample size D itself upon SMA properties. There are very few studies on such SMAs, and those that do exist are insufficient to draw general conclusions. Sutou et al. [13] tested Cu-Al-Mn bamboo structure wires with D between 0.48 and 1 mm, and did not observe obvious differences in σ_{Ms} among these wires. At much smaller scales, sample size effects have been studied by microcompression tests of single crystal pillars. Norfleet et al. [22] showed that in the first test cycle, a 5 μm NiTi pillar had almost the same σ_{Ms} but higher reverse transformation stresses as compared to a 20 μm NiTi pillar, and suggested that the smaller pillar might have less substructure to restrain the reverse transformation; the results averaged over multiple cycles, however, did not exhibit apparent size effects. In the work of Frick et al. [23, 24], critical stresses for both forward and reverse transformations in NiTi pillars decreased as D was reduced from ~2 to ~1 μm; when D further decreased into the submicron regime, the superelastic behavior gradually diminished. On the other hand, San Juan et al. [25, 26] showed that Cu-Al-Ni pillars with $D \approx 1.7$ and 0.9 μm exhibited complete superelastic recovery, far better than the Ni-Ti pillars of similar sizes [23, 24]. Furthermore, both σ_{Ms} and $\Delta E/E$ in the Cu-Al-Ni submicron pillar were reported to be much higher than their counterparts in bulk single crystals of the same composition; the increase in σ_{Ms} was attributed to the paucity of martensite nucleation sites, and the increase in $\Delta E/E$ to the release of elastic transformation strains at the pillar surface and the resulting delay in the reverse transformation [26].

Between small single crystal pillars (< ~20 μm) [22-26] and large diameter wires (> ~500 μm) [12-17, 20, 21] described above, there is a large gap in scale (20–500 μm) that is unstudied in SMAs with $d \approx D$. These scales are in a particularly interesting range for both manufacturing and applications. Here we study the effects of sample size upon the phase transformations underlying SMA properties in polycrystalline Cu-Al-Ni microwires with diameters between 20 and 500 μm and with a bamboo structure. Maximizing the lateral grain size in each wire significantly reduces the brittleness of this class of SMA, which allows us to explore superelasticity, shape memory effects, and hysteresis in Cu-Al-Ni polycrystalline SMAs with very small diameters.

2. Wire Preparation and Characterization

Our experimental Cu-Al-Ni shape memory microwires are fabricated from Cu-13.7Al-5Ni (wt%) alloy. According to Refs. [25, 27], in bulk single crystals of this alloy, the austenite β phase transforms into and from β' (18R) martensite upon cooling and heating, respectively, at transformation temperatures of M_s = 18°C, M_f = 0°C, A_s = 12°C, A_f = 30°C. The corresponding thermal hysteresis ΔT (difference between average martensitic and reverse transformation temperatures) is very small and is only about 6°C.

We use a processing route described in detail elsewhere [28]. Briefly, we use the Taylor-wire drawing technique [29, 30], which involves hot-drawing of a softened glass tube containing the alloy melt. We attain various wire diameters by changing the drawing speed, i.e., faster drawing results in finer wires. The as-formed wires are annealed at 850°C for one hour to both austenitize and promote grain growth, and then quenched to retain the austenite. Finally, the glass layer on the wires is removed by immersion in 10% HF aqueous solution. The resulting wires mostly have uniform diameters, and a few of them are shown in Fig. 2(a-c). The stripe features on the wire surfaces are believed to result from glass flow at the interface during the drawing process, and are very common on the present wires. We test the wires in the as-prepared condition without any additional surface treatment. Fig. 2(d-e) show montaged optical micrographs of two cross-sections, which appear tapered because the sectioning plane is slightly off longitudinal. Nevertheless, we observe that the structure in the wires is indeed bamboo, with grain boundaries running across the wire at approximately 90º to the wire axis. These samples are observed below their M_s (discussed below), so these images also reveal martensite plates that span the entire cross-section of the wire.

Fourteen Cu-Al-Ni microwires with diameters ranging from 466 down to 23 μm are used in the present study, with twelve of them having diameters smaller than 100 μm. These wires are labeled according to their diameters in descending order, e.g., wire #1 has $D \approx 466$ μm while #14 has $D \approx 23$ μm (see Table I). Most of these tested wire segments are very light, e.g., less than one milligram, because of their small diameters. In order to measure their transformation temperatures, we collect them into four groups (#1, #2-3, #4-7, #8-14), each of sufficient mass to exhibit transformation signals in a differential scanning calorimetry (DSC) scan. We run DSC cycles at a heating/cooling rate of 8°C/min using the Q10 apparatus from TA Instruments. The DSC results are shown in Fig. 3, where the biggest wire has transformation temperatures and thermal hysteresis very similar to those mentioned above for bulk single crystals of the same alloy composition. The transformation temperatures for smaller wires seem to shift to higher temperatures, by as much as ~25°C. This increase could in principle be caused by minor

compositional variation (by ≤ 0.1wt% [27, 31]) among the wires. However, given that these samples are all processed directly from a melt of the same composition, such a unidirectional shift in composition with wire size is not expected. Composition measurements on some cross-sections by energy-dispersive spectroscopy showed no variations to within the accuracy of measurement (±1 at% using a calibrated system). The increase in transformation temperatures in smaller wires may be explained as a size effect that is also revealed in our mechanical tests, as shall be seen later in Section 3.

We characterize superelasticity and shape memory properties of the wires in tension using a dynamic mechanical analyzer equipped with a closed furnace (DMA Q800 from TA Instruments, with a maximum force of 18 N). Each end of the wire is mounted in a plastic compound at the two gripping ends and then clamped mechanically. The free (gauge) length varies between 2-6 mm for different wires. The cross-head displacement is measured by a high resolution linear optical encoder within the instrument. Since the M_s temperatures of the wires are around or above ambient temperature (cf. Fig. 3), each wire is partially or fully martensitic before the mechanical tests. After we apply a small preload (corresponding to a stress below 3.5 MPa) to a mounted wire and slowly increase the temperature inside the furnace, the wire contracts notably due to the transformation from martensite to austenite, until the temperature approaches the austenite finish temperature A_f. A_f determined this way for each wire is presented in the last column in Table 1, and it is generally higher in smaller wires; this is consistent with the DSC results shown in Fig. 3. Superelasticity is then revealed by isothermal uniaxial tensile tests at constant loading rate above A_f, and the present Cu-Al-Ni wires are expected to transform into β' martensite under stress (in contrast to the $\beta \rightarrow \gamma'$ transformation observed when the stress is applied at temperatures below A_f [32]).

Some of the wires are also subjected to thermal cycling under constant tensile load, revealing stress-assisted two-way shape memory effects (see Table 2). A procedure similar to that used by Wada and Liu [33] is employed. After mounting a wire and closing the furnace, we reduce the temperature inside to below the martensite finish temperature M_f so that the wire becomes fully martensitic. The load is then increased to the desired magnitude and is held at that value. The wire is then heated to above A_f, and subsequent thermal cycling under the same static load yields a hysteretic curve (similar to Fig. 1(c)) demonstrating two-way shape memory.

3. Superelasticity and Size Effects

All fourteen wires exhibit recoverable superelasticity in tensile tests above their respective austenite finish temperature A_f. The test results are summarized in Table 1, where the critical stresses have been defined in Fig. 1. To lay out the general trends observed, we begin in the following section with two exemplar responses, for a large wire and a small one, that frame the subsequent discussion.

3.1. Superelasticity in large vs. smaller wires

Fig. 4(a)-(d) show the true stress–strain curves for the largest diameter wire in the present study (#1 with $D \approx 466$ μm and $A_f \approx 40$°C), tested up to the maximum load (18 N) of the instrument at 30, 40, 50, and 60°C, respectively. Because the temperature is raised prior to this entire set of tests to identify A_f, the wire is austenitic before the first test. In Fig. 4(a), austenite transforms into martensite upon loading at 30°C, resulting in a large strain of 5.8%, which however only recovers partially after unloading (solid green curve) since the reverse transformation is not complete below A_f. During the subsequent test cycle plotted as a dashed black line, the wire remains mostly martensitic. The test curves at 40°C are plotted in Fig. 4(b), where the reverse transformation occurs down to zero stress and the transformation strain of over 5% barely recovers after unloading; this is consistent with A_f of the wire being close to 40°C (as suggested by the DSC results in Fig. 3). At 50°C, as shown in Fig. 4(c), the recoverable strain remains similarly large, while the stresses for both forward and reverse transformations have increased as compared to those at 40°C. In Fig. 4(d), the overall strain appears much smaller at 60°C, because at this temperature the maximum load allowed by the instrument is not sufficient to trigger full transformation. At each of the latter three temperatures, which are all above A_f, the stress-strain curves for two consecutive mechanical cycles overlap closely.

The true stress-strain curves for a much smaller wire (#13 with $D \approx 26$ μm and $A_f \approx 60$°C) tested at 62, 70, 78, and 86°C are shown in Fig. 4(e)-(h), respectively. Since all tests are carried out above A_f, strain caused by martensitic transformation during loading always completely recovers after unloading, and the maximum recoverable strain approaches 7% in each case. At each temperature, the curves for two consecutive cycles overlap each other, indicating the reproducibility of the superelasticity in this small wire. Again the stresses for both forward and reverse transformations increase with temperature as expected.

Bulk polycrystalline Cu-Al-Ni SMAs usually undergo brittle intergranular fracture during martensitic transformation, due to stress concentration or incompatibility at grain boundaries and triple junctions [34, 35]. In contrast, both wires whose stress-strain curves are shown in Fig. 4 survived multiple complete cycles of martensitic transformation because of their specific grain structure, which contains no triple junctions and therefore reduces transformation incompatibilities. The superelastic behaviors of these wires resemble those of single crystalline Cu-Al-Ni specimens [31, 32].

From Fig. 4, we extract the martensite onset stress σ_{Ms}, the average martensite transformation stress σ_M, and the average austenite transformation stress σ_A at each temperature for each wire. Here σ_M and σ_A are calculated mainly for the purpose of determining the average stress hysteresis in the transformation regime later, but they may also be regarded as an average critical transformation stress over different grains in a wire. The extracted values of σ_{Ms}, σ_M, σ_A (in MPa) are plotted against the testing temperature T (in °C) in Fig. 5. Consistent with the Clausius-Clapeyron relationship [31],

$$\frac{d\sigma}{dT} = -\frac{\Delta H}{T\varepsilon} \tag{1}$$

with ΔH and ε the transformation enthalpy and strain, respectively, the data points for each of these stresses fall on a line for each wire. The best-fit equations of these lines are $\sigma_{Ms} = 2.6(T\text{-}26)$, $\sigma_M = 2.3(T\text{-}20)$, and $\sigma_A = 2.9(T\text{-}31)$ for the large wire with $D \approx 466$ μm, and $\sigma_{Ms} = 2.8(T\text{-}35)$, $\sigma_M = 2.9(T\text{-}25)$, and $\sigma_A = 3.6(T\text{-}49)$ for the smaller wire with $D \approx 26$ μm; for each of these equations the units of σ are MPa and the units of T are °C. These linear equations are plotted in Fig. 5 as solid lines, and their slopes ($\partial\sigma_{Ms}/\partial T$, $\sigma_M/\partial T$, $\partial\sigma_A/\partial T$) are all included in Table 1. It is worth noting that the intercept of the line σ_{Ms} with the x-axis (as shown by the dashed extension of the black lines in Fig. 5) has shifted to a higher temperature in the small wire as compared to that in the large wire, which is consistent with the upward shift in the transformation temperatures revealed by the DSC measurements in Fig. 3.

We observe in both Fig. 4 and Fig. 5 that the smaller wire exhibits a much larger average stress hysteresis $\Delta\sigma = \sigma_M - \sigma_A$ of about 42-61 MPa, as compared to only about 11-18 MPa for the large wire. It is difficult to directly ascertain whether this increase in $\Delta\sigma$ is due to an increase in σ_M or a decrease in σ_A, since the two wires have different transformation temperatures and are tested at different temperatures. If we mentally extrapolate the σ_M and σ_A lines for the large wire in Fig. 5 to higher temperatures (not shown) and compare with the lines for the small wire, it seems that σ_M has increased slightly while σ_A has decreased to a greater extent in the small wire.

3.2. Size effect in stress hysteresis

The above observation of increased average stress hysteresis $\Delta\sigma$ in the smaller wire is actually generally observed in the full series of tested wires. Fig. 6 shows the true stress-strain curves for wires with a range of diameters: 90 μm in (a), 74 μm in (b), 31 μm in (c), and 23 μm in (d). The green (solid) and black (dashed) lines in each plot represent two consecutive tests at a temperature about ten degrees above their respective austenite finish temperature A_f. The stress axes in Fig. 6(a-d) are all at the same scale, so it can be directly seen that the loading and unloading curves separate more widely as the wire diameter decreases, revealing an increase in $\Delta\sigma$. The average transformation stresses, σ_M and σ_A, of these wires are plotted as filled circles and squares, respectively, against the testing temperature T in Fig. 6(e). The blue and red lines in Fig. 6(e) are constructed to cross the data points for the 90 μm wire with a

slope of 2.76 MPa/K (the mean of the $\sigma_M/\partial T$ and $\partial\sigma_A/\partial T$ columns in Table 1); they represent a straightforward Clapeyron extrapolation and provide the expected transformation stresses at other temperatures for this wire. We now compare the measured transformation stresses for other smaller wires with those expected from the 90 μm wire. The 74 μm wire reveals an increase in σ_M and the 31 μm wire a decrease in σ_A, while the small wire with a diameter of 23 μm shows both. Thus Fig. 6(e) shows that an increased $\Delta\sigma$ can possibly result from both an increase in σ_M and a decrease in σ_A, which is consistent with Fig. 5.

In Fig. 7(a), we plot the average stress hysteresis $\Delta\sigma$ as a function of wire diameter D for all wires tested. For large wires above about 100 μm, $\Delta\sigma$ is low and is in the range of 10-20 MPa. This matches well with tensile measurements in the literature on millimeter-scale Cu-Al-Ni single crystals, as captured by the triangular data point at the right of Fig. 7(a) taken from Ref. [32]. The size effect in stress hysteresis, i.e., an increase in $\Delta\sigma$ with decreasing D, emerges gradually at sizes of ~100 μm and below. The critical size of $D \approx 100$ μm here is similar to the critical grain size $d \approx 100$ μm below which a grain size effect begins to appear on the martensitic transformation in bulk polycrystalline SMAs [2-8]. It is intriguing that these two physically very different cases (D is to free surfaces while d is to grain boundaries) exhibit similar critical sizes around 100 μm. This suggests that both types of size effect may originate from a crossover with an intrinsic length-scale characteristic of the martensitic transformation, e.g., a critical size for martensite nuclei or a length scale associated with the elastic field around martensitic regions.

The stress hysteresis $\Delta\sigma$ for the smallest wires with D close to 20 μm is many times (i.e., ~3-7 times) higher than those for the largest wire, and approaches the large stress hysteresis from micro-compression of single crystalline Cu-Al-Ni pillars with diameters 0.9 and 1.7 μm reported in Refs. [25, 26] (shown as square data points on the left of Fig. 7(a)). It was pointed out by Ye et al. [36] that micro-compression tests may involve a contribution from phase transformations occurring in the substrate beneath the tested pillar, which could present an artifact in measuring $\Delta\sigma$. However, since the present wire experiments do not involve any issue of substrate effects, the consistency between our data and pillar compression results suggest that the substrate effect is probably insignificant or at least very subtle in the measured hysteresis for pillar. The present results thus support the interpretation of a genuine sample size effect for pillars in Refs. [25, 26].

Fig. 7(b) shows $\Delta\sigma$ as a function of D in double-logarithmic fashion. A power-law fit of all the data points for the present wires results in $\Delta\sigma \propto D^{-0.49}$, which is plotted as the solid line. The triangular data point for the large single crystal with D = 1.5 mm from Ref. [32] seems to deviate from this fitted line, consistent with a plateau (illustrated by the dashed line) at large sizes, e.g., above ~100 μm. A second fitting of all data points for present wires excluding those for the biggest wire with $D \approx 466$ μm (since this diameter seems to lie in the plateau regime) leads to $\Delta\sigma \propto D^{-0.66}$ (not shown). At the smallest sizes, the literature

results from pillar microcompression also deviate from the solid line of power law scaling, which indicates that there might be another plateau at very small sizes, e.g., below ~10 μm, as illustrated by the dashed line on the left of the figure.

Fig. 7(a-b) exhibit some scatter on the vertical axis partly because they include data for each wire tested at multiple different temperatures, where the measured stress hysteresis values $\Delta\sigma$ can be slightly different from one another (see, e.g., Fig. 4 and 5). To eliminate such minor temperature effects from the scaling analysis, we now determine a single characteristic value of $\Delta\sigma$ for each wire and assemble them in Fig. 7(c). Specifically, we use $\Delta\sigma$ at a temperature ten degrees above the austenite finish temperature A_f. When this value is not directly available in Table 1 for some wires, we extrapolate it by performing a Clapeyron linear fit (not shown) to the existing data in the stress-temperature space (similar to Fig. 5). The data corrected for temperature in this way are less scattered (Fig. 7(c)), but show size dependence very similar to the raw data in Fig. 7(b), with a similar power-law fit of $\Delta\sigma \propto D^{-0.54}$. If there were no size effect, the corrected hysteresis would have been the same for different wires, since other factors that can cause the shift in transformation temperatures (such as composition change) would not change the hysteresis [27]. As a result, we conclude that the variation of stress hysteresis shown in Fig. 7(c) among wires of different diameters speaks to a true size effect.

A size scaling exponent close to one half is relatively common in polycrystalline plasticity, including, for example, the grain size exponent in the Hall-Petch strength scaling relationship. However, the exponent in the present case of superelasticity in SMA wires likely results from different underlying physical mechanisms. Interestingly, some earlier works on the grain size effect in bulk polycrystalline SMAs found that the martensite start temperature $M_s \approx T_{s0} - k_s d^{-0.5}$ in Fe-Ni-C [2, 4, 37] and Cu-Zn-Al alloys [7], and the martensite start stress $\sigma_{Ms} \approx \sigma_{Ms0} + k_{Ms}(d/D)^{-0.5}$ in Cu-Al-Be cylinders [14]. Although such grain size scaling has not yet been mechanistically explained, the similarity of these exponents with the present sample size scaling exponent supports our prior speculation that both types of size effects might relate to a similar critical length scale associated with martensite formation.

3.3. Energy dissipation

As mentioned in the Introduction, the area within the hysteresis loop, ΔE, in the superelastic stress-strain curve is the energy dissipated per unit volume in a superelastic cycle. The fractional energy dissipation $\Delta E/E$, with E the maximum strain energy, is a measure of the energy dissipation or damping capacity. The values of both ΔE and $\Delta E/E$ for all of the present tests are provided in Table 1. The values of $\Delta E/E$ for many of the small wires exceed 40%, which is a very high ratio of energy dissipation.

However, neither ΔE nor $\Delta E/E$ is a proper parameter for comparing between the damping capacities of the different wires here. $\Delta E/E$ decreases significantly with temperature even for the same wire due to the increase in E (in other words, due to the increase in martensitic transformation stresses); for example, it decreases from 54% to 24% when the temperature increases from 62 to 86°C for wire #13, as shown in Fig. 4(e-h) and Table 1. Meanwhile, ΔE is substantially affected by the maximum strain achieved, which is different among the wires. Accordingly, we normalize ΔE by the maximum strain to obtain the characteristic energy dissipation per unit strain, i.e., $\Delta E_{1\%}$. As shown in Fig. 8, there is a strong positive linear correlation between $\Delta E_{1\%}$ and the average stress hysteresis $\Delta\sigma$ for all tests summarized in Table 1; these parameters are essentially equal to within experimental error. This result is intuitively expected, as both parameters are measures of the transformation hysteresis and both are strain-averaged. An even better collapse might be expected if the strain normalization were based on only the transformation strain.

As $\Delta\sigma$ is more straightforward to observe than $\Delta E_{1\%}$, but correlates with it precisely (Fig. 8), it may be used as a legitimate measure of the energy damping capacity of a wire for the present purposes. As a strain-averaged quantity, $\Delta\sigma$ is a more reliable measure of the energy dissipation than the difference between the forward and reverse transformation stresses at one fixed strain used previously in the studies on Cu-Al-Mn [13] and Cu-Al-Be wires [14], since the latter can vary considerably as a function of the strain at which they are measured, particularly in polycrystalline SMAs. With the new insights gleaned from Fig. 8, we can now assert that the results in Fig. 7, which show a size dependence of $\Delta\sigma$, also directly speak to a size effect in energy dissipation.

4. Shape Memory Effect

In addition to isothermal tensile tests that reveal superelasticity, we also perform thermal cycling under static constant load (approximately constant stress) to study the stress-assisted two-way shape memory effect. Results extracted from these tests are summarized in Table 2, where the critical transformation temperatures under finite stress are denoted as T_{Ms}, T_{Mf}, T_{As}, and T_{Af} (defined in Fig. 1(c)) to distinguish from those (M_s, M_f, A_s, A_f) for stress-free transformations defined in Fig. 1(d). T_M and T_A denote the average martensitic and reverse transformation temperatures, respectively, and $\Delta T = T_A - T_M$ is the average temperature hysteresis.

Fig. 9(a) shows some typical thermal cycling curves obtained from wire #13 with $D \approx 26$ μm under approximately static stresses of about 10, 39, and 78 MPa; these results are acquired after the same wire was previously subjected to the isothermal tensile tests shown in Fig. 4(e-h). Under stress, the wire elongates when transforming into martensite upon cooling, and shrinks when transforming back into austenite upon heating. The strain caused by one transformation is completely recovered by the other, verifying the two-way shape memory effect. The maximum recoverable true strain increases slightly with

an increase in applied stress, from 5.5% at 10 MPa, to 6.6% at 39 MPa, and to 7.1% at 78 MPa, which are all comparable to the superelastic strains of 6.3% - 6.8% of this same wire shown in Fig. 4(e-h). Recoverable strains of such a large magnitude have rarely been attained in polycrystalline Cu-Al-Ni SMAs before, largely because of the brittleness of these SMAs. The present bamboo structure wire is much less prone to brittle intergranular fracture, and shows cyclic superelasticity and shape memory effect with large recoverable strains.

In Fig. 9(a), all of the transformation temperatures increase (i.e., curves shift rightwards) with applied static stress, consistent with the Clapeyron relationship of Eq. (1). We extract the average transformation temperatures, T_M and T_A, as well as the martensite start temperature T_{Ms}, and plot them as a function of the applied stress σ in Fig. 9(b) using hollow data points. Since direct thermal measurement on the wire surface is very challenging for such a small wire, the present temperature is measured by a thermocouple located about a centimeter from the wire in the furnace. We use a very low ramping rate, 1°C/min, to minimize measurement error and also provide error bars on the extracted temperatures in Fig. 9(b) to reflect the expected thermal lag at this rate. Also included in Fig. 9(b) are the same solid data points seen previously in Fig. 5, obtained from isothermal superelasticity tests on the same wire. The data from the two types of tests align well, and have essentially the same Clapeyron slopes $\partial\sigma/\partial T$ within experimental error. Such consistency is expected if the same type of transformation (i.e., $\beta \leftrightarrow \beta'$) is triggered in superelasticity and in shape memory (see the diagram schematized in Fig. 1(a)). (Otherwise, if the specimens had transformed into γ' below A_f and into β' above A_f, we would expect a significant change in the slope, i.e., $(\partial\sigma/\partial T)_{\beta \rightarrow \gamma'}$ / $(\partial\sigma/\partial T)_{\beta \rightarrow \beta'} \approx 2$ according to Refs. [32, 38].)

The stress-temperature ($\partial\sigma/\partial T$) slopes from constrained thermal cycling for three other wires (#3, 5, and 10) are also calculated and provided in Table 2, and they range from 1.5 to 3.2 MPa/K. The stress-temperature slopes from superelasticity for these three particular wires are not available for comparison, since only a single isothermal tensile test was conducted on each of them (see Table 1). But the slopes measured from superelasticity tests on other wires in Table 1 are similar to the slopes assessed above for shape memory. We also note in passing that in both Table 1 and Table 2, there are some variations among the $\partial\sigma/\partial T$ slope values, which we believe arise from the limited number of data points (usually two and at most four in the best cases) used for extracting the slopes (although sample size may have some effect on these slopes as well). Nonetheless, the slopes are scattered around the expected range of 2-3 MPa/K for $\beta \leftrightarrow \beta'$ transformation in Cu-Al-Ni single crystals [32, 38], with an average of 2.8 MPa/K in both Table 1 and Table 2.

The other important parameter in Table 2 is the temperature hysteresis $\Delta T = T_A - T_M$, which is about 20°C for most wires. No obvious difference in ΔT is observed between the seven wires in Table 2, probably because of the relatively large uncertainty in the temperature measurement (~±4°C) during thermal

cycling. Nevertheless, ΔT around 20°C for the present wires is significantly higher than the small hysteresis of 6-10°C [27] exhibited by bulk Cu-Al-Ni single crystals of the same composition. Since $\Delta\sigma = (\partial\sigma/\partial T)\Delta T$ according to Eq. (1), an increase in the temperature hysteresis ΔT in smaller samples agrees with the increase in the stress hysteresis $\Delta\sigma$ observed previously.

5. Origins of Size Effects in Shape Memory Alloys

In previous sections, we have shown that the transformation stresses (in superelastic tests) or temperatures (in shape memory tests) shift with a change in the diameter of Cu-Al-Ni shape memory alloy wires. Here we briefly discuss possible origins of such size dependence from a thermodynamic perspective. Since the transformation stresses and temperatures are directly correlated by the Clapeyron relationship of Eq. (1), either may be analyzed to illuminate both. Here we focus on analyzing transformation stresses and energy dissipation during isothermal uniaxial tensile tests above A_f, which reveal the superelastic effect. We first evaluate the plausibility of various size-related contributions to the shift of the transformation stresses, and further specifically discuss those that may underlie the increase in stress hysteresis.

During the transformations between austenite and martensite under an external stress σ, the Gibbs free energy density of the sample changes at the rate

$$\dot{G} = \left[\Delta G_{ch} + \gamma_i A_i + \Delta\gamma_{sf} A_{sf} + E_{el}\right]\dot{f} + E_{fr}\left|\dot{f}\right| - \sigma\dot{\varepsilon} \tag{2}$$

In Eq. (2), the strain rate $\dot{\epsilon} > 0$ and the rate of martensite volume fraction change $\dot{f} > 0$ during forward transformation, while during reverse transformation $\dot{\epsilon} < 0$ and $\dot{f} < 0$. $\Delta G_{ch} = G_{ch}^{M} - G_{ch}^{A} = \Delta H - T\Delta S$ is the change in chemical free energy per unit volume at temperature T, and is positive when $T > A_f$ since austenite is more stable at such temperatures in the absence of stress; superscripts "M" and "A" denote martensite and austenite properties, respectively. γ_i is the interfacial energy per unit area and A_i is the interfacial area density. $\Delta\gamma_{sf} = \gamma_{sf}^{M} - \gamma_{sf}^{A}$ is the difference in surface energy per unit area of martensite and austenite, and multiplies the specific sample surface area A_{sf}. E_{el} is the average increment in the elastic energy density as a result of the transformation. The change in chemical energy, interfacial energy and surface energy, as well as the stored elastic strain energy due to forward transformation are all recovered during reverse transformation, when $\dot{f}$ in Eq. (2) changes its sign. E_{fr} is the irreversible part of the free energy change, and is usually ascribed to the moving interfaces dissipating energy as "frictional work" [39]. Most of E_{fr} is dissipated as heat [40], while part of it may also be emitted as acoustic waves [41].

In Eq. (2), the surface energy term is usually neglected in bulk samples but can in principle play a role in small samples. Other terms may exhibit sample size dependencies as well, although we are not aware of

detailed or quantitative discussion of such issues in the literature. Therefore we consider that the size dependence of the transformation stresses may originate from a sample size dependence of (i) the interfacial energy density, (ii) the difference between the surface energy of austenite and martensite, (iii) the stored elastic energy associated with martensite formation, (iv) acoustic emission as a possible dissipation mechanism, (v) heat transfer which not only is the major dissipation mechanism but also affects the local temperature, and (vi) the magnitude of internal friction itself. In what follows, we discuss each of these terms briefly, estimate the magnitude of the size effect that might emerge from them, and identify the most plausible sources of the size effects seen in our experiments.

(i). Interfacial energy

The interfacial energy density γ_i of twin boundaries among martensite variants is only about 0.02 J/m^2, while that for phase boundaries between austenite and martensite is roughly around 0.5-1 J/m^2 [42, 43]. Therefore the major contribution to the interfacial energy term $\gamma_i A_i$ in Eq. (2) originates from the phase boundaries. Considering the morphology of martensite plates spanning across the sample cross-section as is the case here, the interface density A_i is simply N/H, where N is the total number of phase boundaries during transformation in the sample of height H, and A_i reduces to zero after a full transformation. Thus the magnitude of total interfacial energy is not affected by the sample diameter D.

Additionally, we notice that the interfacial energy is considerably smaller than other energy terms. For example, if we take γ_i = 1 J/m^2 and A_i = 10^4 - 10^5 /m (the variation in A arises from the coalescence of martensite plates during transformation), $\gamma_i A_i$ is then equal to 10^4 - 10^5 J/m^3 (equivalent to 0.075 - 0.75 J/mol for Cu-Al-Ni SMAs). This is several orders of magnitude lower than the transformation enthalpy of ~267-389 J/mol [31, 38] for Cu-Al-Ni SMAs. For these reasons, we conclude that the effect of interfacial energy on transformation stresses should be very limited or even trivial, and is insensitive to sample size.

(ii) Surface energy

The surface energy changes upon martensitic transformation, and such change normalized by volume is captured by the term $\Delta\gamma_{sf}A_{sf}$ in Eq. (2). Since surface energy can be considered as energy needed to break bonds in order to create the surface, γ_{sf}^{M} may be imagined to be somewhat higher than γ_{sf}^{A} due to denser packing (as a result of slight volume contraction [32]). Meanwhile, the surface area per unit volume, A_{sf}, is equal to $4/D$ in fibers, and is much larger in wires with smaller diameter D. As a result, $\Delta\gamma_{sf}A_{sf}$ is positive, and is larger in smaller wires. It tends to increase both σ_M and σ_A, and the resulting shift in these transformation stresses is larger in smaller wires. However, σ_M and σ_A for a wire are shifted by the same amount, so the average stress hysteresis $\Delta\sigma$ (= σ_A - σ_M) cannot be altered by the surface

energy change; in other words, the surface energy variation upon transformation may contribute to the size dependence of the transformation stresses, but not to the size effect in hysteresis.

However, since the surface energies of metallic materials are generally very small, e.g., around 1-3 J/m^2 [44], $\Delta\gamma_{sf}$ should be below 1 J/m^2. Accordingly, the $\Delta\gamma_{sf}A_{sf}$ term is no more than ~4/D J/m^3 (e.g, when D = 100 μm, this term is about 4x10^4 J/m^3 or 0.3 J/mol for Cu-Al-Ni, which is very small compared to the transformation enthalpy of ~300 J/mol). We conclude that this effect only offers a very minor, probably almost negligible, contribution to the size effect in transformation stresses observed in Section 4.

An additional effect of surface on martensitic transformation relates to the heterogeneous nucleation of martensite at free surfaces. It has been recognized that a homogeneous nucleation model [45] for martensitic transformation results in a nucleation energy barrier prohibitively high [40]. The nucleation of martensite is therefore believed to be heterogeneous, and occurs at microstructural defects including grain boundaries and free surfaces. At least in the present wires, the surfaces are sufficiently rough to envision heterogeneous nucleation there being especially favorable, and to preclude a paucity of nucleation sites on surfaces as a factor for the observed size effects. In smoother specimens or micro-pillars, the effect on nucleation may be more pronounced [26]. However, as long as nucleation can occur at surfaces, the energy barrier for such heterogeneous nucleation should be similar in different wires, and so this is not likely to underlie the size effect on hysteresis.

(iii) Stored elastic energy

The solid-state martensitic transformation proceeds by dilatation and shear of the original austenite lattice. The change in volume and shape of a transformed region must be accommodated by its surrounding austenite or other martensite variants. This results in elastic mismatch stresses in both martensite and austenite (partial plastic accommodation by slip is neglected for thermoelastic transformations). The stored elastic energy, i.e., E_{el}, affects the forward and reverse transformation stresses as shown in Eq. (2).

Eshelby solved the elastic field for the case where an ellipsoidal region undergoes a distortion inside an infinite matrix [46]. However, when the shear transformation occurs in a matrix of finite size, the stress distribution is different from the Eshelby solution, and by extension so is the elastic energy. Here we address the Eshelby problem in a finite matrix in order to elucidate the possible sample size dependence of the elastic energy term. Specifically, we conduct a simple plane strain calculation using the commercial finite element solver ABAQUS. The transforming region is an ellipse with an aspect ratio of eight, embedded in a two-dimensional elastic wire matrix, as shown in Fig. 10. The ellipse is oriented at 45° to the axis of the wire; its size is fixed, with its horizontal width D_0 = 20 μm. The wire height H is fixed at a large value of 150 μm, while the width D of the wire is varied between D_0 and 7.5D_0 in a series of

calculations intended to reveal the sample size effect. We apply a stress-free pure shear $\gamma = 0.02$ to the ellipse in the sense that causes tension along the sample axis, and allow the sample to relax by partitioning elastic stresses into the ellipse and surrounding matrix. For these calculations, a Young's modulus of 26 GPa, Poisson's ratio of 0.466, and shear modulus of 95 GPa are used, which are extracted from the stiffness matrix of austenite in Cu-Al-Ni SMAs reported in Ref. [47].

Fig. 10(a-e) shows some of our calculation results as contours of elastic energy density (in MJ/m^2), which generally increases with sample size and reflects the stress state. For the smallest diameter of $D = D_0$ in Fig. 10(a), the mandatory shear results in a surface step and thus the internal stresses are quite low. In Fig. 10(b) and (c) where $D = 1.2D_0$ and $1.5D_0$, respectively, the transformed region no longer contacts the free surfaces, but the elastic fields still interact substantially with the surfaces. As a result, the internal stresses only increase moderately in these two cases. When D further increases to $3D_0$ in Fig. 10(d) and $6D_0$ in Fig. 10(e), the shear applied inside the embedded ellipse is no longer considerably relieved by the free surfaces. Internal stresses thus develop significantly in both the ellipse and the matrix, and approach those predicted by the Eshelby solution for an infinite matrix.

Consistent with the above observations, the total strain energy in the sample, E_{total}, is observed to increase with D, and gradually saturates for $D > 4D_0$, as shown in Fig. 10(f). Here for simplicity we take the total strain energy of the largest system ($D = 7.5D_0$) as E_∞, and plot the ratio of the total strain energy E_{total} of a relaxed system to E_∞, as a function of normalized sample size D/D_0. E_{total} for the smallest sample with $D = D_0$ is 31.81 μJ, only about 16% of the saturated value E_∞ of 194.59 μJ. If the total area affected by the shear is assumed to be twice that of the transforming region, the above two E_{total} values correspond to an average energy density of 0.20 MPa and 1.24 MPa, respectively. The difference between these two energy densities is ~1.04 MPa, or 0.26 MPa per 1% shear, which produces a stress difference of 26 MPa. Meanwhile, the average strain energy densities inside the transformed area for these two cases are ~0.10 MPa and ~0.87 MPa, respectively. The difference between them is ~0.77 MPa, or 0.19 MPa per 1% shear, which corresponds to a stress difference of 19 MPa and is very close to the previous estimation of 26 MPa.

In summary, the calculations surrounding Fig. 10 overall suggest that the stored elastic energy resulting from an internal shear distortion becomes much smaller as the sample dimension is reduced. As a result, the transformation stresses σ_M and σ_A in small wires could be decreased by as much as ~20 MPa compared to those of large samples or bulk materials, considering the factor of stored elastic energy alone. This magnitude is significant when compared with the experimentally assessed critical stress shifts (which are estimated at about 20-50 MPa; cf. Fig. 5 and 6e). As a caveat, we note that the above calculations are basically schematic, and for the effect seen here to be observed in practice would essentially require that martensite domains form with a characteristic size independent of sample size.

Another scenario where a sample size effect may also exist is when the transformed region can always span the entire cross-section of the sample such as the case in Fig. 10(a), and the width (instead of length) of the transformed band becomes the fixed, characteristic length scale. We have performed a series of calculations for this case as well and in this case, relaxation of lattice dilation at free surfaces is also a significant effect in SMAs with small sample volumes.

It was proposed in prior work on Cu-Al-Ni shape memory alloy pillars [26] that stored elastic energy density E_{el} after martensitic transformation is smaller in submicron pillars than in the bulk alloy, and as a result, the reverse transformation is delayed in pillars compared to that in the bulk alloy. Our calculations and discussion above for the present wires are largely in agreement with this viewpoint, i.e., E_{el} is lower in smaller wires. However, we additionally note that the elastic energy term E_{el} serves as an energy barrier for the forward martensitic transformation but as a driving force for the reverse transformation. A decrease in E_{el} tends to promote martensitic transformation and lower the martensitic transformation stress σ_M; meanwhile, since the driving force for the reverse transformation is reduced, the reverse transformation during unloading will be delayed compared to when E_{el} is higher. Therefore σ_A and σ_M both tend to decrease when the wire diameter decreases, considering the factor of elastic energy alone. E_{el} could only affect the average stress hysteresis $\Delta\sigma$ (= σ_A - σ_M) if the E_{el} term in Eq. (2) were different in magnitude during forward and reverse transformations. In our opinion, this is relatively unlikely, since each incremental accumulation of elastic energy during forward transformation is reversibly released during reverse transformation.

(iv) Acoustic emission

As observed in the work of Bonnot et al. [41] as well as by Baram and Rosen [48], acoustic emission accompanies the thermoelastic transformations between austenite and martensite, and it is related to the interaction of propagating interfaces with defects such as dislocations. However, although some energy does leave the specimen in the form of mechanical energy wave, it is believed that this acoustic energy is negligibly small compared to the irreversible heat, and thus is not an important factor for the hysteresis and the associated size effects.

(v) Heat transfer

Heat transfer is an important process during the phase transformations in shape memory alloys, not only because the frictional work E_{fr} is mostly dissipated as heat, but also because such first-order transformations involve the release and absorption of latent heat. Since heat is exchanged between the sample and the environment at the sample surface, the temperature might be different in smaller wires than in bigger ones, since the former have a higher specific surface area.

As a starting point for the analysis, we may quickly rule out a change in dominant heat transfer mechanism as playing any significant role in size effects on shape memory alloys. The Biot number for cylindrical specimens of Cu-Al-Ni with diameter D is calculated as

$$Bi = hL_c / k = Dh / 4k \tag{3}$$

with the volume to surface ratio $L_c = D/4$, thermal conductivity $k \approx 400$ W/(m·K), and the convective heat transfer coefficient $h \approx 10$ W/(m^2·K). Bi is extremely small not only for all of our microwire samples (of order 10^{-7}-10^{-6}), but also for virtually any relevant sample size (e.g., even at D = 1 m, Bi ≈ 0.006). This means that conduction is extremely rapid as compared to the convective loss at the surface for essentially all sample sizes. The temperature within all samples can be taken as uniform, and heat transfer is dominated by the rate of convection.

For a convection-limited kinetic condition, we may explore the sample size effect on the dissipation of heat into the surroundings through a lumped capacitance analysis, i.e., by solving for the temperature evolution from the equation

$$\dot{q} - 4h\left(T - T_\infty\right)/ D - \rho C_p \dot{T} = 0 \tag{4}$$

with q the generated heat, T_∞ the ambient temperature, ρ the density, and C_p the specific heat capacity. We consider the case of constant heat generation rate between t = 0 and t_0, i.e., $\dot{q} = Q_{tot} / t_0$. Here t_0 represents the time span for transformation, and thus is inversely proportional to the loading or strain rate. Q_{tot} can be considered the total heat resulting from the transformation latent heat and the irreversible dissipation of frictional work. To focus on the effect of heat transfer in this section, we for the moment assume $E_{fr}^{A\to M}$ and $E_{fr}^{M\to A}$ each to be 5% of the latent heat 330 J/mol (4.4x10^7 J/m^3) [39], and Q_{tot} becomes Q_F = 4.62x10^7 J/m^3 and Q_R = -4.18x10^7 J/m^3 for forward and reverse transformation, respectively. The solution to Eq. (4) during $0 \le t \le t_0$ is

$$T(t) = T_\infty + \frac{Q_{tot}}{\rho C_p} \cdot \frac{\tau}{t_0}\left[1 - \exp\left(-\frac{t}{\tau}\right)\right] \tag{5}$$

and the cumulative heat dissipation per unit volume as a function of time is

$$Q(t) = \frac{Q_{tot}}{t_0}\left\{t - \tau\left[1 - \exp\left(-\frac{t}{\tau}\right)\right]\right\} \tag{6}$$

The thermal time constant τ in Eqs. (5) and (6) is defined as

$$\tau = D\rho C_p / 4h \tag{7}$$

With ρ = 7140 kg/m^3 and C_p = 440 J/(kg·K), τ is approximately $7.85\times10^4 D$ s; that is, τ is about 157 s when D = 2 mm, 15.7 s when D = 200 μm, and 1.57 s for D = 20 μm.

The temperature evolution calculated from Eq. (5) and the heat lost to the environment as predicted by Eq. (6) are respectively plotted in Fig. 11(a) and (b), using t_0 = 60 s and $Q_{tot} = Q_F$, for wire diameters ranging from 2 mm down to 20 μm. By the end of forward transformation, i.e., when $t = t_0$, the temperature rises by over 10 K in the 1 and 2 mm wires, because heat is dissipated at a very low rate in these big wires due to their larger thermal constant τ. The temperature rises much less in smaller wires, and remains nearly constant (only increases by ~0.38 K) in the smallest wire with 20 μm diameter. This is further corroborated by Fig. 11(b) which shows that for this smallest wire the heat is dissipated at approximately the same rate as it is generated, i.e., $Q(t) \approx \dot{q}t$; in other words, heat generated is almost instantaneously dissipated. The y-axis of Fig. 11 would simply be reversed if heat is absorbed, so the same conclusions (smaller temperature excursions and faster heat transfer by convection in smaller wires) also apply to the reverse transformation.

To quantitatively evaluate the effect of heat transfer on the transformation behaviors, we invoke the first law of thermodynamics in the rate form $\dot{W} = \Delta\dot{U} + \dot{Q}$, where W is the mechanical work, ΔU is the internal energy change, and Q is the heat dissipation.

$$\sigma\dot{\varepsilon} = \left[\Delta H_0 + \rho\Delta C_p\left(T - T_0\right) + \gamma_i A_i + \Delta\gamma_{sf} A_{sf} + E_{el}\right]\dot{f} + \rho\overline{C}_p\dot{T} + 4h\left(T - T_\infty\right)/D \tag{8}$$

Eq. (8) applies to both forward transformation when the strain rate $\dot{\epsilon} > 0$ and the rate of martensite fraction change $\dot{f} > 0$, and reverse transformation when $\dot{\epsilon} < 0$ and $\dot{f} < 0$. In Eq. (8), $\overline{C_p} = (1-f)C_p^A + fC_p^M$, and $\Delta C_p = C_p^M - C_p^A$; $\Delta H_0 = H_0^M - H_0^A$ is the transformation enthalpy at the equilibrium temperature T_0 when $\Delta H_0 = T_0\Delta S_0$, and $\Delta H_0 + \rho\Delta C_p(T - T_0)$ is the actual transformation enthalpy ΔH at temperature T. The key is to compare the rate of heat dissipation, $\dot{Q} = 4h(T - T_\infty)/D$, to the rate of heat generation, $\dot{q} = -T\Delta S\dot{f} + E_{fr}|\dot{f}|$, where $\Delta S = \Delta S_0 + \rho\Delta C_p In(T/T_0)$.

We first turn our attention to "classical" size and rate effects associated with sluggish heat transfer in large specimens. When the duration of transformation t_0 is smaller than the thermal constant τ defined in Eq. (7), as is the case for mm-scale shape memory wires transforming under fast loading rates, $\dot{Q}$ is much lower than $\dot{q}$, and T changes significantly during the transformations (see Fig. 11). For these large wires, the stress hysteresis $\Delta\sigma$ measured at high loading rate is larger than that obtained with slower loading [32]. This increase in $\Delta\sigma$ has been attributed to the temperature hysteresis (i.e., $T^{A\to M} > T_\infty$ and $T^{M\to A} < T^{A\to M}$) developed as a result of fast loading rate, as the two types of hysteresis are related by the Clapeyron relation of Eq. (1). Our analysis of Eq. (8) above offers additional insights into this rate effect. For large wires transforming at fast rates, the dissipation is very small, and the transformation stresses are mainly affected by the temperature via the thermal energy term $\rho\bar{C}_p\dot{T}$. Since the heat dissipated to the surroundings and that stored in the material as thermal energy are both supplied by the external mechanical work, what directly affects the hysteresis is the heat generation $\dot{q}$ defined above integrated over transformation time.

$$\left(\sigma^{A\to M}-\sigma^{M\to A}\right)\varepsilon_t = E_{fr}^{A\to M}+E_{fr}^{M\to A}+\int_0^1\left[-\left(T\Delta S\right)^{A\to M}+\left(T\Delta S\right)^{M\to A}\right]df \qquad (9)$$

where ε_t is the total transformation strain. Eq. (9) explicitly expresses the dependence of stress hysteresis on T and ΔS, both of which vary considerably for the scenario in question.

The size effect in the present experiments is not related to the above "classical" effect. It arises under very different conditions, which are defined by $\tau \ll t_0$, which holds for small wires and/or slow tests. Under this condition, all of the heat generated is instantly dissipated, and not only is the temperature in the sample spatially uniform at any instant, the temperature does not rise; $\dot{Q}=\dot{q}, \dot{T}=0, T=T_\infty$. This condition is satisfied for present microwires, which are mostly smaller than 100 μm and have been tested at slow rates (each superelastic cycle takes 3.5-35 minutes); we estimate $\tau/t_0 \approx 0.01-0.1$. In this limiting case, the energy balance in Eq. (8) becomes identical to Eq. (2) written for isothermal conditions, and Eq. (9), which describes the hysteresis, reduces to

$$\left(\sigma^{A\to M}-\sigma^{M\to A}\right)\varepsilon_t = E_{fr}^{A\to M}+E_{fr}^{M\to A} \qquad (10)$$

In Eq. (10), the stress hysteresis only depends on the frictional work, which is indeed widely perceived as the major source of thermodynamic irreversibility that gives rise to the hysteresis for thermoelastic martensitic transformation [39, 40]. Accordingly, we can conclude that the size effect in hysteresis revealed in our shape memory microwires must originate from size dependence of the frictional work itself.

(vi). Internal friction

Frictional work is spent on interface motion during transformations, and is related to the density of obstacles or defects at the transformation front. In the present microwires where martensite plates span the entire wire cross-section and phase boundaries propagate along the wire axis, we envision that the free surfaces provide the main obstacles or pinning points for interface propagation. The smaller the wire diameter D is, the stronger the pinning effect of surfaces may become, degrading more useful mechanical work into frictional work which is then eventually dissipated in the form of heat.

The expected scaling of internal frictional work with D is not entirely clear, although there is a resemblance between the process of jerky interface propagation and a dislocation crossing a grain. The resemblance between these two phenomena has also been recognized in prior studies on the dependence of martensitic transformation temperature M_s on grain size d [4, 7]. As discussed earlier in Section 3.2, the scaling of M_s with d, and the stress hysteresis $\Delta\sigma$ with D studied at present, both exhibit a scaling exponent close to -0.5, the same as the well-known Hall-Petch scaling exponent. In this connection, it is interesting to note that martensitic transformation and dislocation activity involve characteristic length scales significantly different. In the kink band theory for martensitic nucleation [49], the critical elliptical nucleus has a length of ~10 μm and a width of ~100 nm at a stress one thousandth

the shear modulus. The estimated nucleus size on average is about two to three orders of magnitude larger than the Burgers vector of a dislocation. This may help explain why the sample size effect for martensitic transformation becomes evident when the size is decreased only as fine as 100 μm, whereas sample size effects on micropillar strength really emerge only at scales below about 1 μm [50, 51]. What is more, both of these sample size effects are essentially associated with energy dissipation, as plastic deformation is simply one of the dissipation mechanisms with the strength being the "stress hysteresis".

While the sample size effect on $\Delta\sigma$ can plausibly be linked to the pinning of interfaces at free surfaces, this line of reasoning does not explain why there is an apparent plateau in the hysteresis in Fig. 7 at small sizes, between 20 and 1 μm. It is important to note that this apparent plateau separates two different sets of experiments (microwire vs. micropillar testing) with some key differences: one is the testing mode and the other is the sample surface condition. Data for the present microwires are obtained from uniaxial tension testes while those for the pillars are obtained from uniaxial compression. Tension-compression asymmetries exist in shape memory alloys [52], and may have a scale dependence. Also, the present microwires are tested in the as-prepared, rough surface condition as can been seen in Fig. 2, while the pillar surfaces are very smooth since they are polished by the focused ion beam at very low currents [26]. Rougher surfaces may provide more resistance to interface motion through the presence of more local pinning points, and thus more frictional work has to be performed to propagate the interfaces through the wires than pillars of the same size. On the other hand, the pillars still have very large hysteresis despite their smooth surfaces, suggesting that the enhanced hysteresis cannot only be due to a surface roughness effect.

One other interesting feature of the present size effect further differentiates it from the "classical" size effect caused by slow heat transfer in large samples. The frictional work effects described above are not expected to exhibit any significant rate effects, provided we remain under conditions where the sample experiences no thermal excursion. We have tested the rate dependence of some of our wires to verify this expectation. For example, revisiting Fig. 4(e-h), which shows superelastic test data for the 26 μm wire (with $\tau \approx 2\,\mathrm{s}$), we now emphasize that the two cycles shown were conducted at different rates. The solid green data points were collected at approximately 11 MPa/min (i.e., transformation time $t_0 \approx 200$ s), while the hollow data points in black were collected during a test roughly an order of magnitude faster at 110 MPa/min (i.e., $t_0 \approx 20$ s). No rate dependence on the stress-strain curves can be discerned. This is in stark contrast to results at comparable rates in large (mm-scale) rods of the same material, where the classical rate effect on hysteresis is observed [32]. This corroborates our prior analysis that the present size effect in hysteresis is not caused by loading rates or heat transfer, but rather is a new effect inherent to the martensitic transformation. This is also consistent with the origin for hysteresis being internal friction, which is not anticipated to have a rate-dependence.

(vii) Summary of sample size effects in SMAs

To briefly summarize the above discussion, we have been able to rule out some potential contributions to the sample size effects we have seen in our experiments on SMAs. Specifically, interfacial and surface energy terms as well as acoustic emission are believed to be essentially insignificant to the main results in this paper. The sample size effect on the critical stresses for the martensite and austenite transformations are quite likely affected by the role of free surfaces in relaxing transformation elastic strains, which can explain transformation stress shifts of perhaps one to two dozens of MPa. However, elastic relaxation cannot explain the size effect on hysteresis because of its reversibility.

There are two size effects on hysteresis: one of these is a "classical" effect that applies to larger samples generally above about 1 mm in size, and the second is a new effect relevant to smaller specimens of the kind tested here. We schematically distinguish these different size effects in Fig. 12. The classical size effect is due to slow heat exchange between a large sample and its environment. During transformation there is a significant thermal excursion in the sample, which leads to shifts in the transformation stresses and a change in the hysteresis (see Eq. (9)). Because slow heat transfer is responsible, this size effect involves increased hysteresis for *larger* samples, and has strain-rate dependence because faster tests lead to more heat accumulation. These two trends are captured by the red lines in Fig. 12. The diameter above which this size effect emerges depends on the loading rate as well; the slower the rate, the larger this critical diameter becomes. In contrast, the second size effect occurs in samples that are sufficiently small to exchange heat with the surroundings very quickly. They can efficiently shed/absorb heat during transformations and thus do not undergo any thermal excursion. In this case, we can point to a size effect on internal friction as the reason why smaller samples have a larger hysteresis. Interestingly, this new effect does not exhibit rate dependence, as shown by the convergence of the two black curves in Fig. 12. Accordingly, the critical size below which this new size effect is expected to occur should also be largely independent of rate, and is probably determined by some intrinsic length scale characteristic of martensitic transformation (e.g., the critical nuclei size).

6. Conclusions

We have fabricated microwires of Cu-Al-Ni shape memory alloys with a wide range of diameters, and processed them to form a bamboo-type grain morphology. Our thermomechanical tests show that this strategy is very effective at suppressing the intergranular fracture common in polycrystalline Cu-Al-Ni alloys, since the present wires exhibit cyclic superelasticity and shape memory behaviors with large recoverable strains. As a result, we have been able to systematically study the effects of sample size (wire diameter) on shape memory and superelastic properties.

A major result of the present work is that we observe size effects in the transformation temperatures, stresses, and hysteresis in these SMAs. As the wire diameter decreases below about 100 micrometers, the transformation temperatures increase (the austenite start and finish temperatures shift more than the martensitic start and finish temperatures); meanwhile, the austenite transformation stresses seem to decrease while the direction of shift in the martensitic transformation stresses is difficult to ascertain. Mostly importantly, the hysteresis and thus the energy dissipation formed by a cycle of martensitic and reverse transformations are found to be significantly larger in smaller wires. This result is in line with prior work that observed very large hysteresis in Cu-Al-Ni submicron pillars as compared to bulk alloys [26], but the present experiments reveal the full range of the transition, which occurs gradually between about 100 and 10 μm. A power law fitting to the stress hysteresis results in a size scaling exponent around -0.5.

The observed size effects may originate from a number of factors, including the interfacial energy, surface energy change, stored elastic energy, mechanical wave propagation, heat transfer, and internal friction. After evaluating each, we favor the stored elastic energy, heat transfer, and internal friction during transformations as the most important factors leading to the size dependence of transformation temperatures and stresses. More specifically, the relief of elastic transformation stresses at free surfaces becomes appreciable, and can potentially explain the shift in transformation temperatures/stresses in smaller specimens. However, since the stored elastic energy is recoverable after reverse transformation, it does not contribute to the size effect in hysteresis and dissipation. While the classical size effect in hysteresis in mm-scale large wires is caused by sluggish heat transfer, we attribute the size effect in the hysteresis of present small microwires to the enhanced internal frictional work during the transformations.

Acknowledgments

We acknowledge the support of the US Army Research Office through the Institute for Soldier Nanotechnologies at MIT. We also appreciate helpful discussions with Professor David C. Dunand at Northwestern University and Professor Jose San Juan at University of the Basque Country, Spain, and acknowledge the experimental involvement of X. Zhang (Northwestern University) in the production of some of the wires.

Reference

[1] Tadaki T, Otsuka K, Shimizu K. Annu Rev Mater Sci 1988;18:25.
[2] Umemoto M, Owen WS. Metall Trans 1974;5:2041.
[3] Ansell GS, Brofman PJ, Nichol TJ, Judd G. The effect of austenite strength on the transformation to martensite in Fe-Ni and Fe-Ni-C alloys. In: Olson GB, Cohen M, editors. International Conference on Martensitic Transformations. Cambridge, MA, 1979. p.350.
[4] Brofman PJ, Ansell GS. Metall Trans A 1983;14:1929.
[5] Hayzelden C, Cantor B. Acta Metall 1986;34:233.
[6] Seki K, Kura H, Sato T, Taniyama T. J Appl Phys 2008;103.
[7] Adnyana DN. Metallography 1985;18:187.
[8] Mukunthan K, Brown LC. Metall Trans A 1988;19:2921.
[9] López del Castillo C, Mellor BG, Blázquez ML, Gómez C. Scripta Metall 1987;21:1711.
[10] Waitz T, Antretter T, Fischer FD, Karnthaler HP. Mater Sci Technol 2008;24:934.
[11] Waitz T, Tsuchiya K, Antretter T, Fischer FD. MRS Bull 2009;34:814.
[12] Sure GN, Brown LC. Metall Trans A 1984;15:1613.
[13] Sutou Y, Omori T, Yamauchi K, Ono N, Kainuma R, Ishida K. Acta Mater 2005;53:4121.
[14] Montecinos S, Cuniberti A, Sepulveda A. Mater Charact 2008;59:117.
[15] Araya R, Marivil M, Mir C, Moroni O, Sepúlveda A. Mater Sci Eng A 2008;496:209.
[16] Somerday M, Wert J, Comstock R. Metall Mater Trans A 1997;28:2335.
[17] Dvorak I, Hawbolt EB. Metall Trans 1975;6:95.
[18] Sawaguchi T, Sato M, Ishida A. Metall Mater Trans A 2004;35:111.
[19] Fu YQ, Zhang S, Wu MJ, Huang WM, Du HJ, Luo JK, Flewitt AJ, Milne WI. Thin Solid Films 2006;515:80.
[20] Sutou Y, Omori T, Koeda N, Kainuma R, Ishida K. Mater Sci Eng A 2006;438:743.
[21] Koeda N, Omori T, Sutou Y, Suzuki H, Wakita M, Kainuma R, Ishida K. Mater Trans 2005;46:118.
[22] Norfleet DM, Sarosi PM, Manchiraju S, Wagner MFX, Uchic MD, Anderson PM, Mills MJ. Acta Mater 2009;57:3549.
[23] Frick CP, Orso S, Arzt E. Acta Mater 2007;55:3845.
[24] Frick CP, Clark BG, Orso S, Sonnweber-Ribic P, Arzt E. Scripta Mater 2008;59:7.
[25] Juan JMS, No ML, Schuh CA. Adv Mater 2008;20:272.
[26] Juan JS, No ML, Schuh CA. Nat Nanotech 2009;4:415.
[27] Recarte V, Perez-Saez RB, Bocanegra EH, No ML, San Juan J. Metall Mater Trans A 2002;33:2581.
[28] Chen Y, Zhang XX, Dunand DC, Schuh CA. Appl Phys Lett 2009;95:171906.
[29] Taylor GF. Phys Rev 1924;23:655.
[30] Donald IW. J Mater Sci 1987;22:2661.
[31] Otsuka K, Sakamoto H, Shimizu K. Acta Metall 1979;27:585.
[32] Otsuka K, Wayman CM, Nakai K, Sakamoto H, Shimizu K. Acta Metall 1976;24:207.
[33] Wada K, Liu Y. Acta Mater 2008;56:3266.
[34] Sakamoto H, Kijima Y, Shimizu K. Trans Jpn Inst Met 1982;23:585.
[35] Miyazaki S, Otsuka K, Sakamoto H, Shimizu K. Trans Jpn Inst Met 1981;22:244.
[36] Ye J, Mishra RK, Pelton AR, Minor AM. Acta Mater 2010;58:490.
[37] Malygin GA. Phys Solid State 2008;50:1538.
[38] Gastien R, Corbellani CE, Sade M, Lovey FC. Scripta Mater 2004;50:1103.
[39] Ortín J, Planes A. Acta Metall 1988;36:1873.
[40] Wollants P, Roos JR, Delaey L. Progr Mater Sci 1993;37:227.
[41] Bonnot E, Vives E, Mañosa L, Planes A, Romero R. Phys Rev B 2008;78:094104.
[42] Stupkiewicz S, Petryk H. ESOMAT: European Symposium on Martensic Transformations 2009:03013.
[43] Stupkiewicz S, Maciejewski G, Petryk H. Acta Mater 2007;55:6292.
[44] Wang X, Jia Y, Yao Q, Wang F, Ma J, Hu X. Surf Sci 2004;551:179.
[45] Olson GB, Cohen M. Scripta Metall 1975;9:1247.
[46] Eshelby JD. Proc Roy Soc London Ser A 1957;241:376.
[47] Sedlák P, Seiner H, Landa M, Novák V, Sittner P, Mañosa L. Acta Mater 2005;53:3643.
[48] Baram J, Rosen M. Acta Metall 1982;30:655.
[49] Frank FC, Stroh AN. Proc Phys Soc London Sect B 1952;65:811.

[50] Greer JR, Oliver WC, Nix WD. Acta Mater 2005;53:1821.
[51] Greer JR, Nix WD. Phys Rev B 2006;73.
[52] Gall K, Sehitoglu H, Chumlyakov YI, Kireeva IV. Acta Mater 1999;47:1203.

Table 1. Summary of superelastic test data for the SMA microwires. The critical stresses σ_{Ms} and σ_{Mf} are the stresses at which austenite starts and finishes the transformation into martensite upon loading, while σ_{As} and σ_{Af} are the start and finish stresses for the reverse transformation during unloading. σ_M and σ_A denote the average stresses for the martensitic and reverse transformations, respectively, and the difference between them is the average stress hysteresis $\Delta\sigma$. ε_{max} is the maximum strain. ΔE is the area within the hysteresis, and E is the maximum strain energy.

Table 1.

Wire	D (μm)	T_{test} (°C)	Critical Stresses (MPa)				Average Stresses (MPa)			ε_{max} (%)	Energy		Slope (MPa/K)			T_{Af} (°C)
			σ_{Ms}	σ_{Mf}	σ_{As}	σ_{Af}	σ_M	σ_A	$\Delta\sigma$		ΔE (MPa)	$\Delta E/E$ (%)	$\frac{\partial \sigma_{Ms}}{\partial T}$	$\frac{\partial \sigma_M}{\partial T}$	$\frac{\partial \sigma_A}{\partial T}$	
#1	466	30	14	35			26.3			5.8			2.6	2.3	2.9	40
		40	31	56	49	0	42.3	24.5	17.8	5.7	1.11	36				
		50	59	91	84	44	70.8	58.8	12.0	5.4	0.63	17				
		60	91			75	94.3	82.9	11.4	2.8	0.41	21				
#2	109	40	17	94	62	0	59.0	23.5	35.5	3.0	1.06	48	3.5	1.5	2.7	40
		50	52	118	100	37	74.0	50.5	23.5	4.3	1.13	32				
#3	90	50	57	86	70	40	69.0	50.7	18.3	6.8	1.29	26				40
#4	83	50	47	86	67	24	64.0	42.0	22.0	1.5	0.28	26	3.5	3.0	2.7	44
		60	82	110	94	63	93.9	69.4	24.5	2.1	0.49	26				
#5	74	60	85	159	102	51	131.0	78.7	52.3	5.5	2.62	37				50
#6	73	50	39	63	45	24	50.9	30.1	20.8	2.5	0.49	40	1.6	2.0	2.3	40
		60	55	80	58	44	70.4	52.9	17.5	3.9	0.77	28				
#7	60	50	66	142	96	41	106.7	71.7	35.0	2.5	0.79	30				40
#8	54	50	43	82	63	0	64.2	33.5	30.7	4.2	1.10	46	1.5	2.6	3.2	50
		55	50	105	78	19	77.8	52.2	25.6	4.7	1.14	35				
		60	58	116	98	30	90.0	65.3	24.7	5.2	1.16	29				
		65	65													
#9	53	49.5	34	67	48	11	49.2	22.6	26.6	2.6	0.56	44	1.3	1.2	1.4	45
		55	40	74	65	19	55.8	26.6	29.2	3.0	0.65	39				
		60	48	81	75	28	62.2	37.0	25.2	2.7	0.48	29				
#10	52	60	56	108	88	18	75.3	46.8	28.5	5.5	1.38	36				53
#11	33	71	42	86	35		64.8			3.4			2	1.4		76
		76	50	93	49	0	71.8	31.5	40.3	3.7	1.29	54				
#12	31	65	74	145	84	23	109.2	41.2	68.0	4.1	2.46	59	2.1	3.5	4.3	60
		70	82	160	113	32	127.0	61.3	65.7	5.1	2.99	53				
		80	105	177	140	54	162.0	105.1	56.9	5.5	2.98	51				
#13	26	62	75	152	72	18	107.1	45.9	61.2	6.3	3.61	54	2.8	2.9	3.6	60
		70	100	167	106	53	129.4	78.8	50.6	6.8	3.25	38				
		78	120	187	133	82	152.2	104.9	47.3	6.9	3.10	30				
		86	143	207	163	109	175.6	133.7	41.9	6.8	2.70	24				
#14	23	70	98	188	132	57	157.6	85.3	72.3	2.4	1.57	46	3.7	4.0	4.9	61
		85	138	283	256	124	227.0	171.8	55.2	3.3	1.72	24				
		100	211			198	279.4	234.0	45.4	1.8	0.59	14				

Table 2. Summary of shape memory test data for the SMA microwires obtained from thermal cycling under constant load (approximately constant stress σ). The critical temperatures have been defined in Fig.1.

Wire	D (μm)	Test σ (MPa)	Test Ramp (°C/min)	Critical Temperatures (±4°C) T_{Ms}	T_{Mf}	T_{As}	T_{Af}	Average Temperatures (±4°C) T_M	T_A	ΔT	ε_{max} (%)	Slope (MPa/K) $\frac{\partial\sigma}{\partial T_{Ms}}$	$\frac{\partial\sigma}{\partial T_M}$	$\frac{\partial\sigma}{\partial T_A}$
#3	90	0.8	5/1/5	23	16	38	46	20	39	19	1.5	1.9	2.5	2.7
		8	5/1/5	26	16	40	47	25	44	19	3.2			
		16	5/1/5	30	17	41	56	25	45	20	4.0			
		32	5/1/5	39	21	47	57	32	51	19	5.1			
#5	74	2.4	5/1/5	32	22	45	53	27	48	21	3.0	1.5	2.5	3.2
		24	5/1/5	46	28	49	63	35	55	20	4.8			
#7	60	0.4	2/1/2	28	18	35	43	23	39	16	2.5			
#9	53	0.05	1	31	17	33	47	21	42	21	2.5			
#10	52	2.4	1.3	37	20	40	60	30	46	16	3.7	1.9	2.7	1.6
		11.8	1.3	40	25	43	65	33	54	21	4.6			
		23.6	1.3	48	30	46	69	38	59	21	5.3			
#12	31	7	1	72	46	64	82	52	74	22	3.4			
#13	26	9.7	1	39	27	48	66	33	55	22	5.5	3.8	3.7	3.7
		38.9	1	48	33	56	72	42	62	20	6.6			
		78	1	57	44	66	77	51	73	22	7.1			

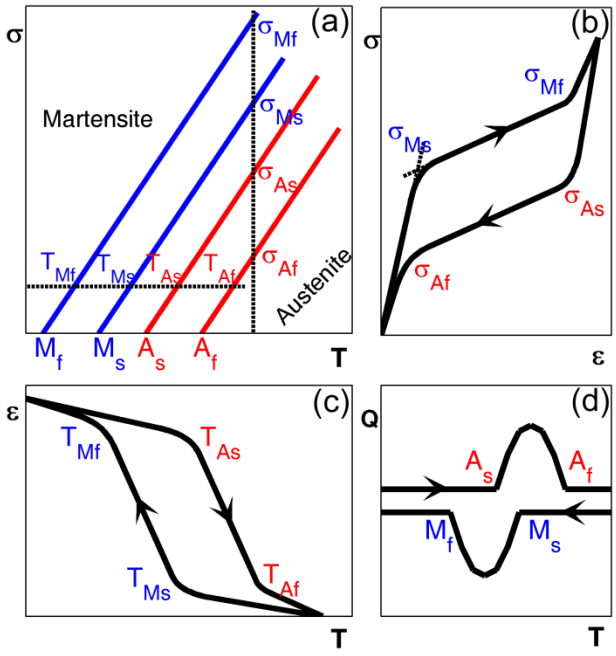

Figure 1. (Color Online) Schematic overview of properties of shape memory alloys measured in this study. (a) The stress-temperature phase diagram for austenite and martensite. (b) Isothermal superelastic stress-strain curve, with transformation stresses defined on the curve. (c) Isostress strain-temperature curve from mechanically-constrained thermal cycling, with stress-dependent transformation temperatures defined on the curve. (d) Heat absorption and release during heating and cooling, respectively, revealed by DSC scan; the initiation and conclusion of each peak defines a critical transformation temperature.

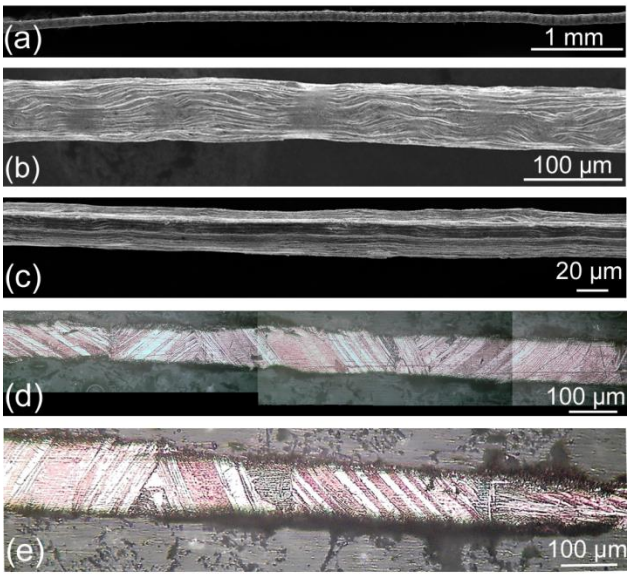

Figure 2. (Color Online) (a-c) Micrographs of some of the Cu-Al-Ni wires with average diameters around 90, 65, 30 µm, respectively. (d-e) Montaged optical micrographs of cross-sectioned wires with diameters around 100 µm, which show bamboo grain structures and also show martensite plates spanning across the wires.

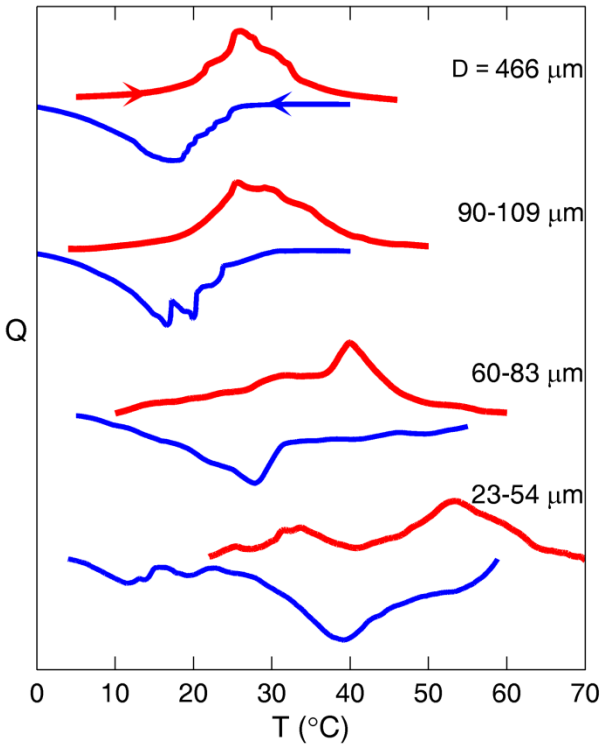

Figure 3. (Color Online) Differential scanning calorimetry scans of Cu-Al-Ni wires with different ranges of diameter *D*. The upper (red) curves are for the endothermic martensite to austenite transformation on heating, while the lower (blue) curves are for the exothermic austenite to martensite transformation on cooling. The y-axis for the heat *Q* absorbed (on heating) or released (on cooling) has been scaled by different magnitudes for different groups of wires in order to show all the peaks clearly in one plot.

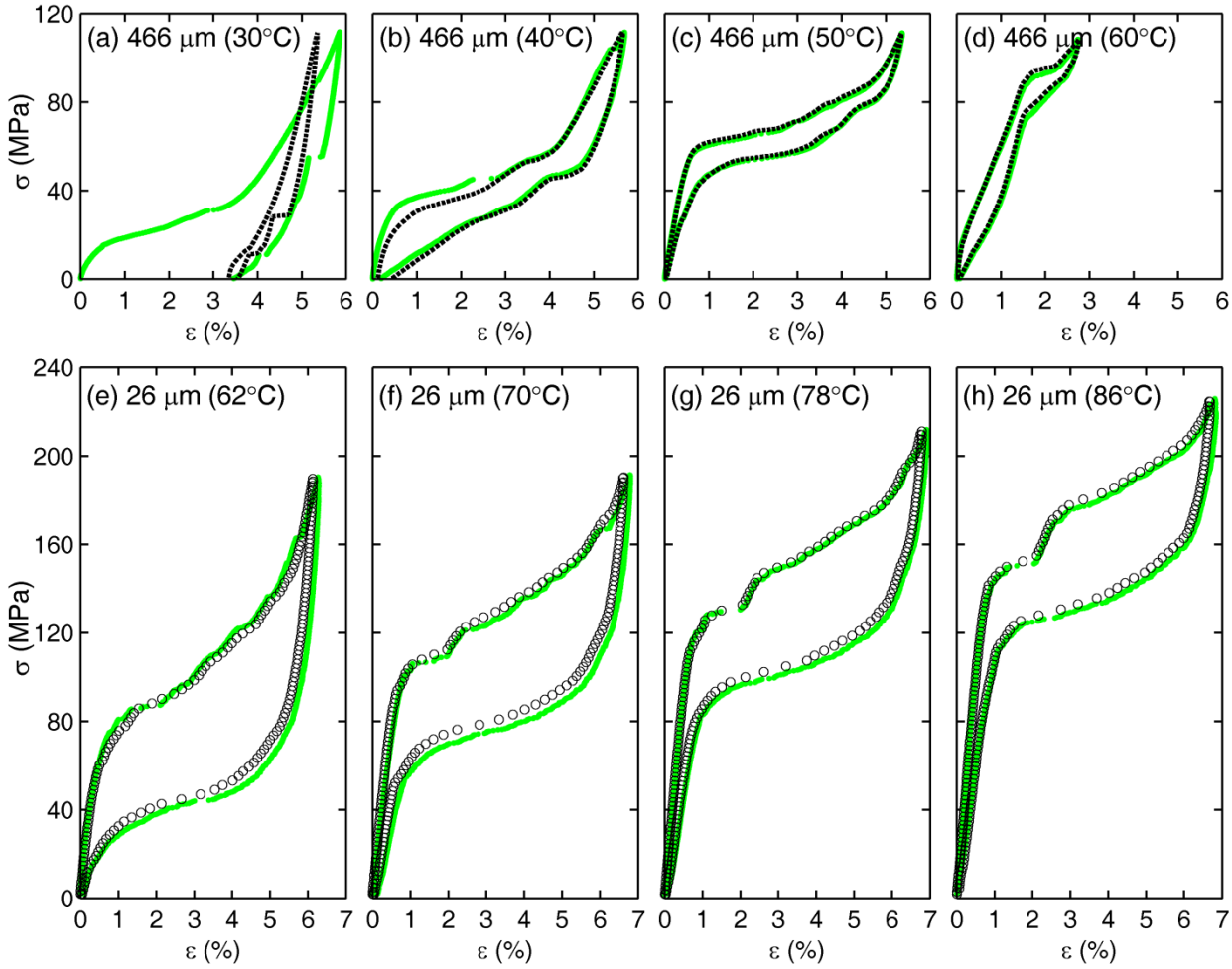

Figure 4. (Color Online) True stress-strain curves for a large wire (a-d) and a small wire (e-h) at various temperatures. At each temperature, two consecutive tests yield consistent results (plotted as points in black and curves in green). For each wire, the transformation temperatures are seen to increase with temperature as expected. Additionally, the hysteresis for the small at all temperatures is in general larger than the hysteresis of the larger wire.

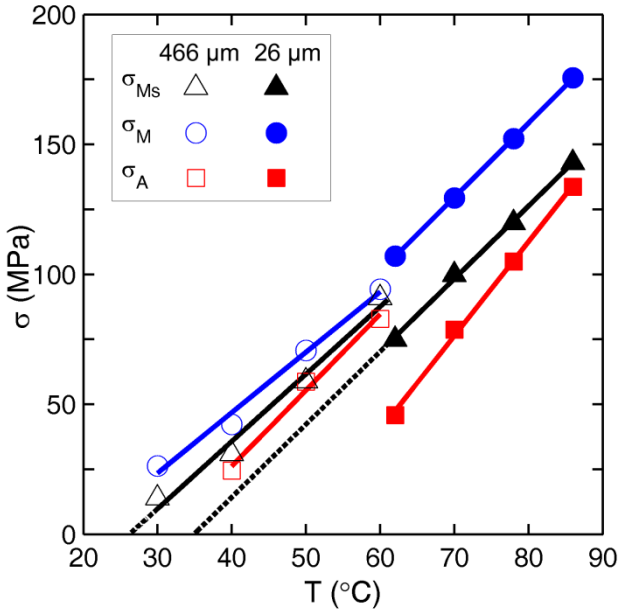

Figure 5. (Color Online) The martensite start stress σ_{Ms}, as well as average transformation stresses σ_M and σ_A, for the 466 μm wire (hollow data points) and the 26 μm wire (solid data points), extracted from tests shown in Fig. 4.

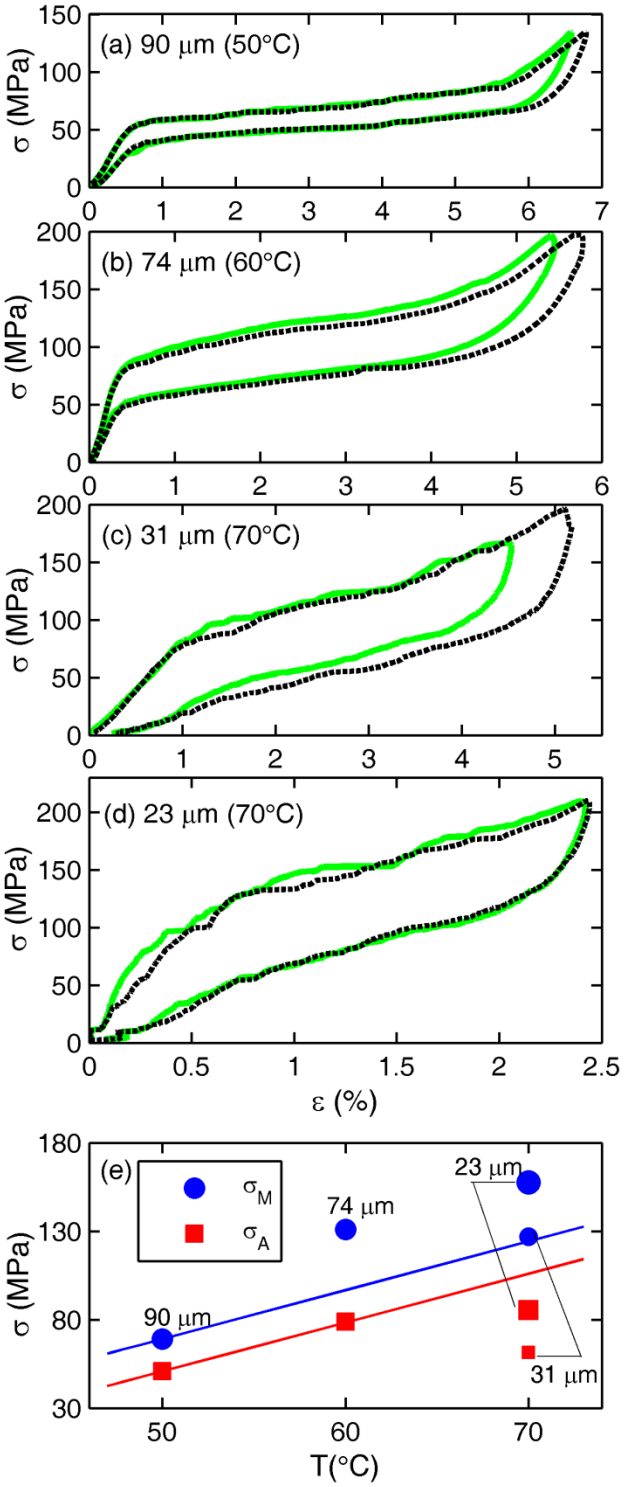

Figure 6. (Color Online) (a-d) Stress-strain curves for four microwires, showing increasing hysteresis with decreasing diameters. The dashed (black) and solid (green) curves are from two consecutive tests. (e) The stress-temperature diagram for these four wires, where the data are collected from curves in (a-d). The lines are the Clapeyron extrapolation of the data for the 90 μm wire to higher temperatures.

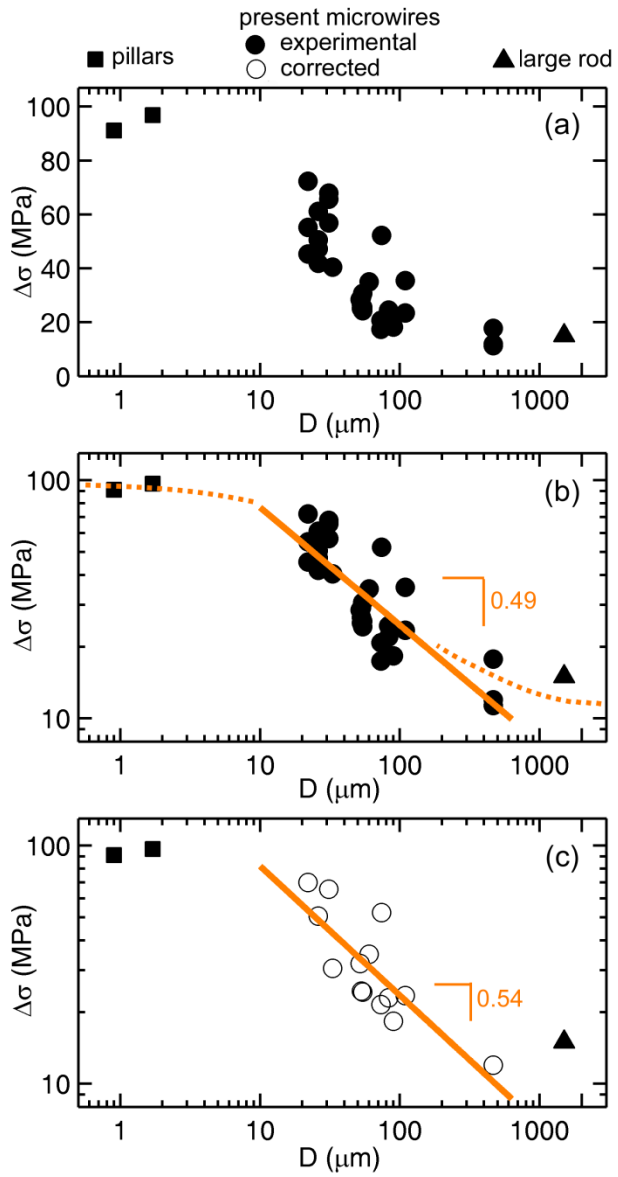

Figure 7. (Color Online) (a) Dependence of the stress hysteresis $\Delta\sigma$ on sample diameter D. The data for micropillars are from Ref. [26] and the data point for the large rod is from Ref. [32]. (b) Size scaling of $\Delta\sigma$ with D, and the fitting as shown by the solid line yields a scaling exponent of 0.49. The dashed lines indicate the possible presence of plateaus in stress hysteresis. (c) Scaling of modified stress hysteresis after correcting the data for temperature effects (all the corrected data are for temperatures 10ºC above A_f).

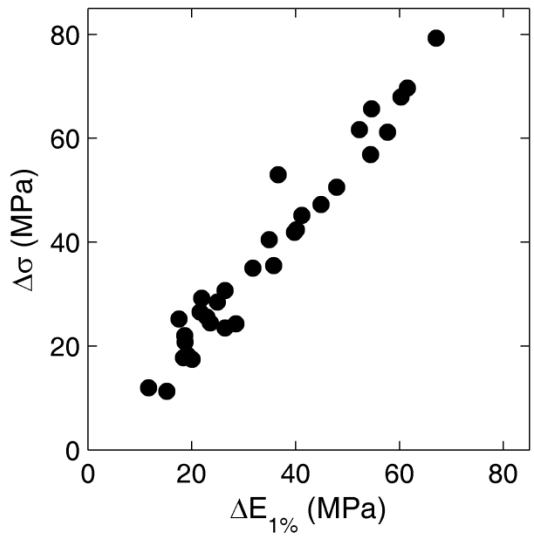

Figure 8. The average stress hysteresis $\Delta\sigma$ and the dissipated energy per unit strain, $\Delta E_{1\%}$, exhibit a strong linear correlation, confirming that $\Delta\sigma$ is a legitimate measure of the energy dissipation.

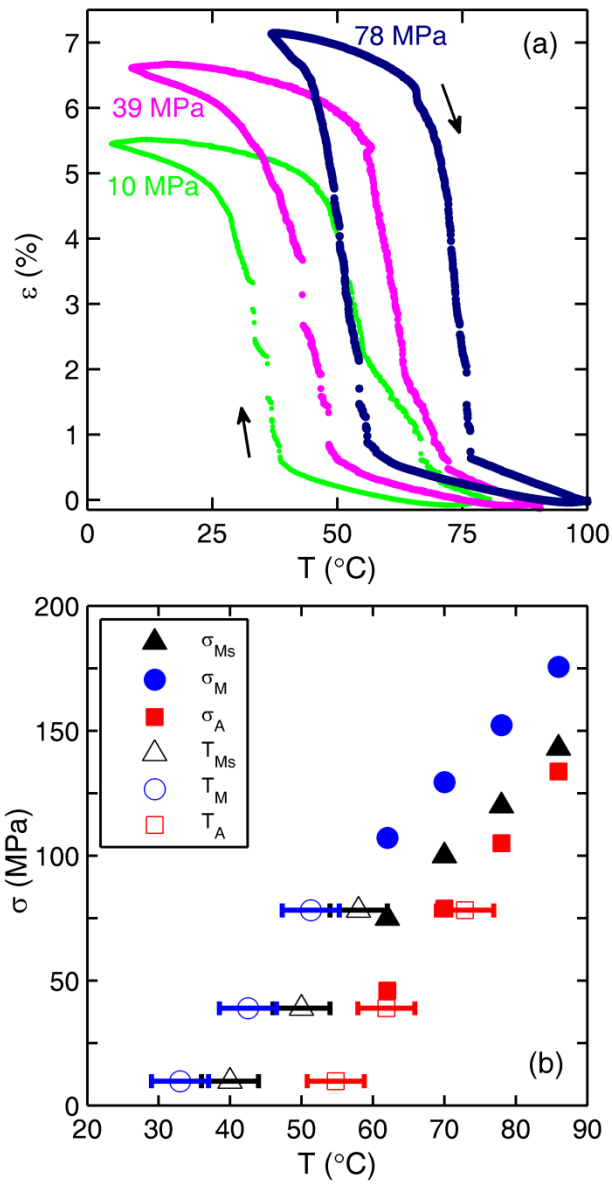

Figure 9. (Color Online) (a) Shape memory properties of a 26 micron diameter wire, revealed by thermal cycling under a constant tensile load. The transformation temperatures shift rightwards with an increase in the applied static stress. (b) The applied stress and the corresponding transformation temperatures extracted from (a) plotted as hollow data points in the stress-temperature space. The solid data points are the transformation stresses of the same wire obtained from isothermal superelastic curves shown in Fig. 4(e-h).

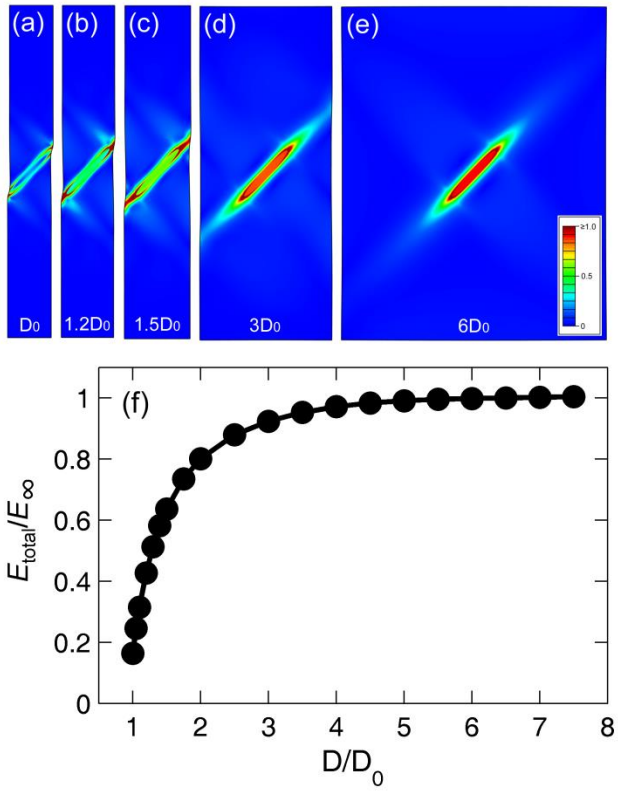

Figure 10. (Color Online) (a-e) Contours of elastic strain energy density after an internal elliptical region of fixed size is sheared by 2%. The strain energy density inside and around the sheared region increases as the sample diameter increases from D_0 to $6D_0$. (f) The strain energy E_{total} of the whole sample normalized by E_∞, approximated by the total strain energy of the sample with diameter $7.5D_0$.

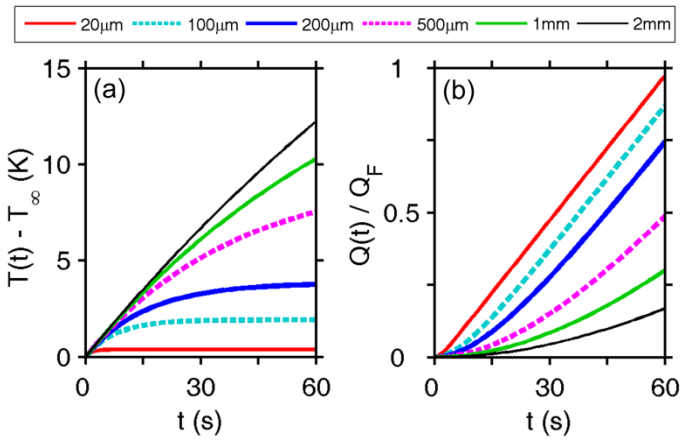

Figure 11. (Color Online) (a) The temperature evolution predicted by Eq. (5), and (b) the total heat dissipation predicted by Eq. (6) for the case of t_0 = 60 s, i.e., the total amount of heat Q_F is generated uniformly in 60 s.

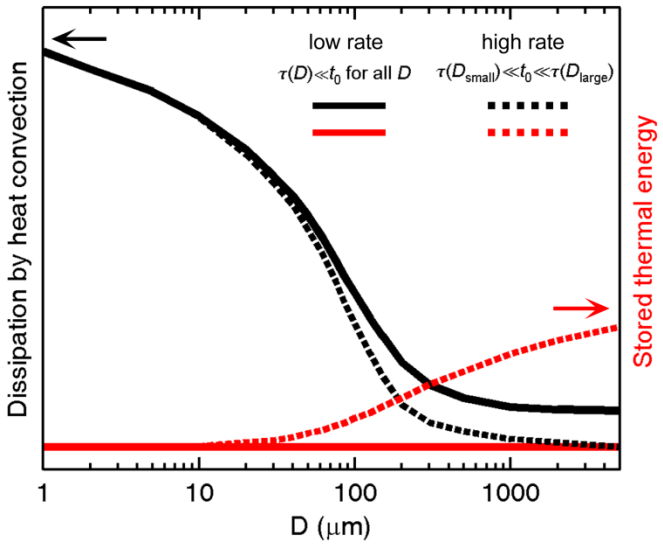

Figure 12. (Color Online) Illustration of two different size effects in shape memory wires based on Eqs. (9) and (10). The classical size effect for mm-scale wires [32] is illustrated by the dashed red line, which shows that at high loading rates the stored thermal energy increases with wire diameter D, causing an increase in hysteresis. This effect disappears when the loading rate is decreased, as shown by the solid red line. The size effect revealed by present microwires is, however, fundamentally different, as shown by the solid black line. Isothermal condition ($\tau(D) << t_0$) is satisfied in these small microwires, and the dissipated heat (equal to the generated heat) increases with decreasing D due to more frictional work in smaller wires. This new size effect does not vanish when the loading rate is changed.